Supporting Information

Korostelev *et al.* 10.1073/pnas.0810953105

SI Materials and Methods

Crystallization. Ribosomes were purified from *Thermus thermophilus* as described (1) with the following modifications. After column chromatography on Toyo-Pearl Butyl 650S, the buffer of the eluted ribosome fraction was replaced with buffer E (25 mM Tris-OAc, pH 7.0, 50 mM KOAc, 10 mM NH_4OAc, 10 mM $Mg(OAc)_2$), using Centricon Plus YM-100 (Amicon). An equal volume of microcrystallization solution (100 mM Tris-OAc, pH 7.0, 200 mM KSCN, 7% PEG20k, 15% PEG200, 2.8% deoxy-BigChap) was then added at room temperature, and the mixture was stored at 4 °C. After a few days, microcrystals were harvested and dissolved in buffer E. The ribosome concentration was adjusted to 20 mg/ml, and stored in aliquots at -80 °C until used for complex formation.

The mRNA M0–27 [GGC AAG GAG GUA AAA AUG UAA AAA AAA] was chemically synthesized (IDT) (1). *Escherichia coli* $tRNA^{fMet}$ was purchased from Sigma-Aldrich. The gene for *T. thermophilus* RF2 lacking T52 from the start codon where a frameshift occurs was cloned into pET24b. RF2 was purified using the same procedure reported for RF1 (1). The 70S:mRNA:$tRNA^{fMet}$:RF2 termination complex was formed as described for the RF1 complex (1), using the molar ratios 1:2:2.4:4, respectively. Crystallization and cryoprotection procedures were as described (1).

x-ray data collection and structure determination. Crystals were screened at beamlines 7.1, 9.1, 9.2 and 11.1 at the Stanford Synchrotron Radiation Laboratory, and at beamline 4.2.2 at the Advanced Light Source, Lawrence Berkeley National Laboratory. x-ray diffraction data were recorded at beamline 23 ID-D at the Advanced Photon Source at Argonne National Laboratory using an x-ray wavelength of 0.9537 Å and an oscillation angle of 0.2°. Data from four datasets obtained from different positions of the same crystal were integrated and merged using the XDS package (2), scaled in SCALA (3) and truncated in TRUNCATE (4). 1% of reflections were marked as test-set (R^{free} set) reflections to monitor the progress of refinement.

Structure determination started with rigid-body refinement of the previously determined structure of the RF1 termination complex, which was obtained from the same crystal form (1). At this stage of refinement, release factor was not included in the structure. Secondary structure elements and some side chains of RF2 were visible in the starting Fourier difference maps (Fig. S3). The 1.8 Å structure of free *E. coli* RF2 (5) was modified to fit the difference map obtained after rigid-body refinement. The sequence was modified to that of *T. thermophilus RF2* employing T-COFFEE (6) and MODELLER (7). The 2.5 Å structure of free *T. thermophilus* RF2 (8) was used as an aid in modeling several flexible parts of the release factor. After simulated annealing and B-factor refinement in CNS (9), the structure of the RF2 termination complex was subjected to TLS refinement in PHENIX (10), yielding good stereochemistry and crystallographic statistics (Table S2). NCS restraints were used throughout the refinement as described (1). PYMOL (11), O (12) and local real-space refinement (13) were used for model building. Figs. were rendered using PYMOL (11).

1. Laurberg M, *et al.* (2008) Structural basis for translation termination on the 70S ribosome. *Nature* 454:852–857.
2. Kabsch W (1993) Automatic processing of rotation diffraction data from crystals of initially unknown symmetry and cell constants. *J Appl Crystallogr* 26:795–800.
3. Evans P (2006) Scaling and assessment of data quality. *Acta Crystallogr D* 62:72–82.
4. CCP4 (1994) The CCP4 suite: Programs for protein crystallography. *Acta Crystallogr D Biol Crystallogr* 50:760–763.
5. Vestergaard B, *et al.* (2001) Bacterial polypeptide release factor RF2 is structurally distinct from eukaryotic eRF1. *Mol Cell* 8:1375–1382.
6. Notredame C, Higgins DG, Heringa J (2000) T-Coffee: A novel method for fast and accurate multiple sequence alignment. *J Mol Biol* 302:205–217.
7. Eswar N, *et al.* (2007) Comparative protein structure modeling using MODELLER. *Curr Protocols Protein Sci* Chapter 2, Unit 29.
8. Zoldak G, *et al.* (2007) Release factors 2 from Escherichia coli and Thermus thermophilus: structural, spectroscopic and microcalorimetric studies. *Nucleic Acids Res* 35:1343–1353.
9. Brunger AT, *et al.* (1998) Crystallography & NMR system: A new software suite for macromolecular structure determination. *Acta Crystallogr D* 54:905–921.
10. Adams PD, *et al.* (2002) PHENIX: Building new software for automated crystallographic structure determination. *Acta Crystallogr D* 58:1948–1954.
11. DeLano WL (2002) The PyMOL Molecular Graphics System (Delano Scientific, Palo Alto, CA).
12. Jones TA., Zou JY, Cowan SW, Kjeldgaard M (1991) Improved methods for building protein models in electron density maps and the location of errors in these models. *Acta Crystallogr A* 47 (Pt 2):110–119.
13. Korostelev A, Bertram R, Chapman MS (2002) Simulated-annealing real-space refinement as a tool in model building. *Acta Crystallogr D* 58:761–767.

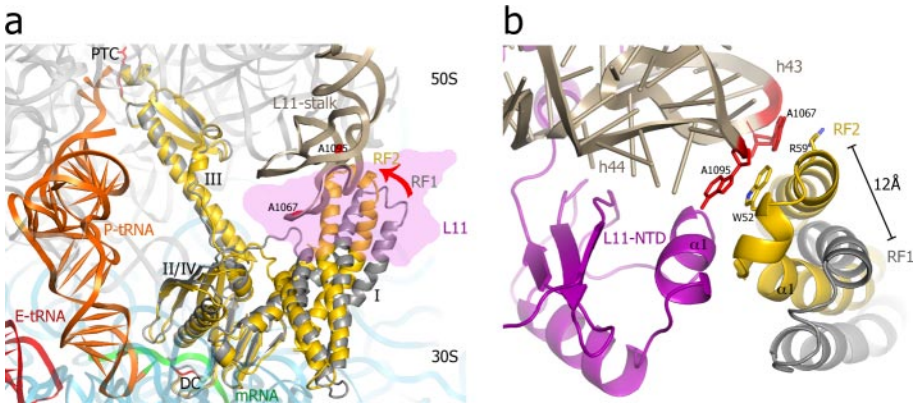

Fig. S1. Interactions between domain 1 of RF2 and the L11 stalk of the 70S ribosome. (*a*) Superposition of the RF1 (1) and RF2 (this work) termination complexes demonstrates that unlike RF1 (gray), RF2 (yellow) contacts the L11 stalk. (*b*) Helices α2 and α1 of RF2 interact with h43 and h44 of 23S rRNA (gray) and with the proline-rich helix α1 of L11 (magenta), respectively. The quality of the electron density map in this region permits only limited interpretation of the details of the interactions between RF2 and L11.

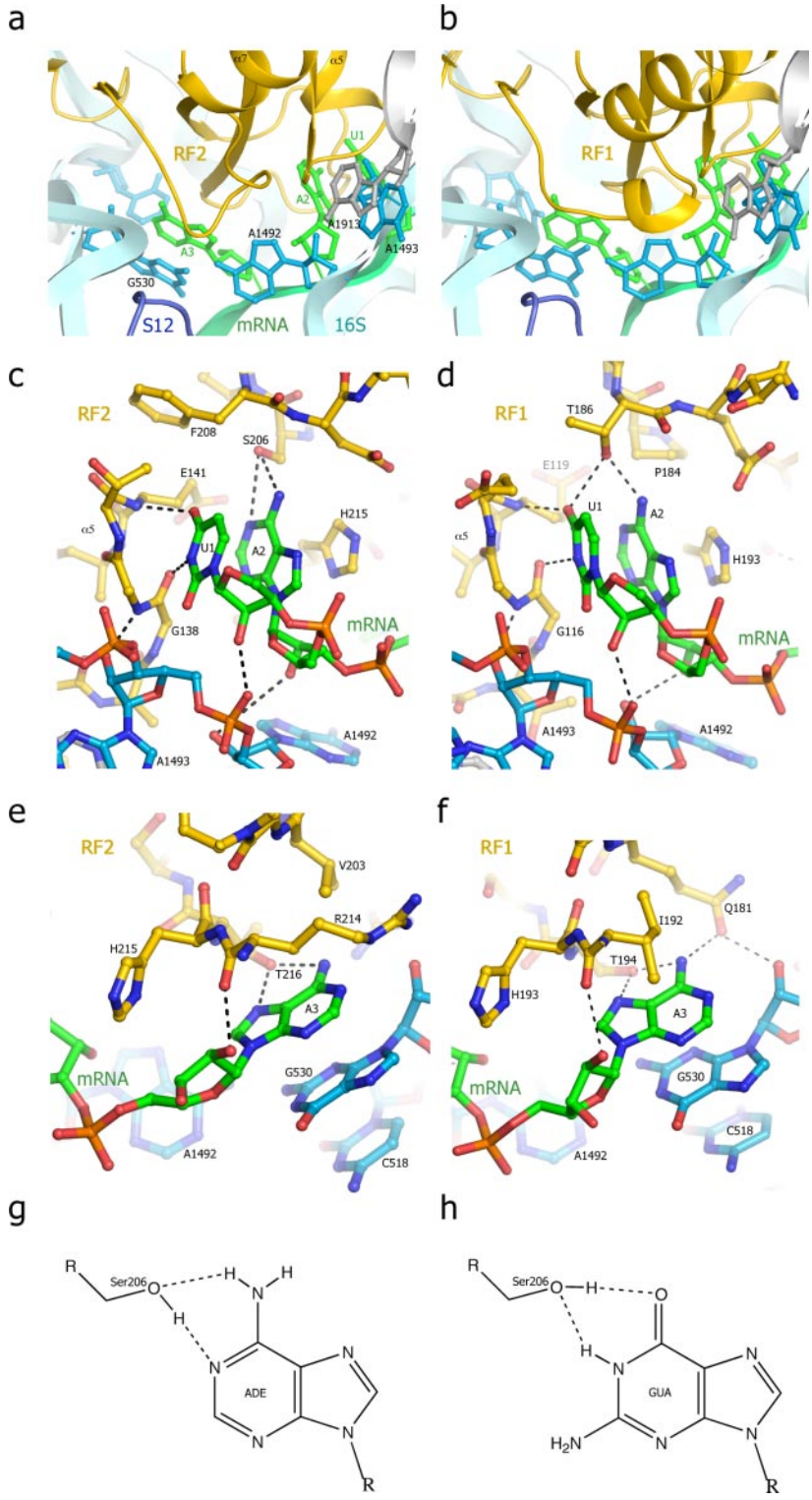

Fig. S2. Codon recognition by RF2 (this work) and RF1 (1). (*a* and *b*) Overall view showing the similarity between the conformations of mRNA (green), nucleotides G530, A1492 and A1493 of 16S rRNA (cyan) and A1913 of 23S rRNA (gray) in the RF2 and RF1 termination complexes. (*c* and *d*) Recognition of U1 and A2 of the UAA stop codon by RF2 and RF1, respectively. (*e* and *f*) Discrimination of the third base (A3) by RF2 and RF1, respectively. (*g* and *h*) A model for recognition of adenine and guanine at the second position of the stop codon by the conserved Ser-206 of RF2.

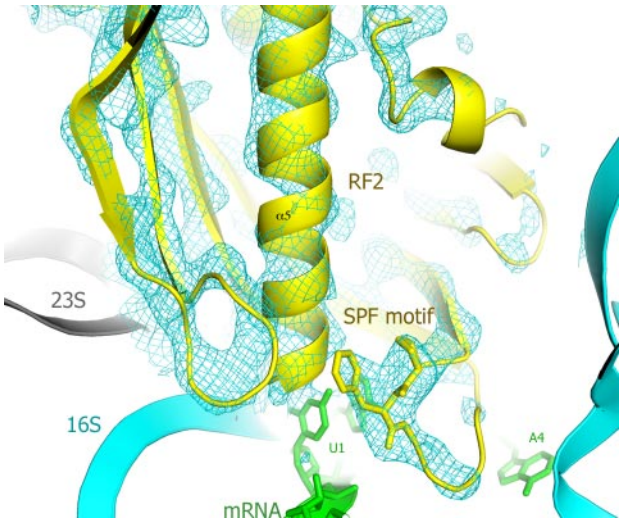

Fig. S3. Unbiased σ_A-weighted $3F_{obs}$-$2F_{calc}$ electron density map calculated before inclusion of RF2 into the model. Proline and phenylalanine side chains of the fully conserved SPF motif implicated in recognition of the stop codon can be unambiguously identified in this initial map (cyan). The final refined model for RF2 (yellow), mRNA (green), 16S (cyan) and 23S (gray) rRNA is shown.

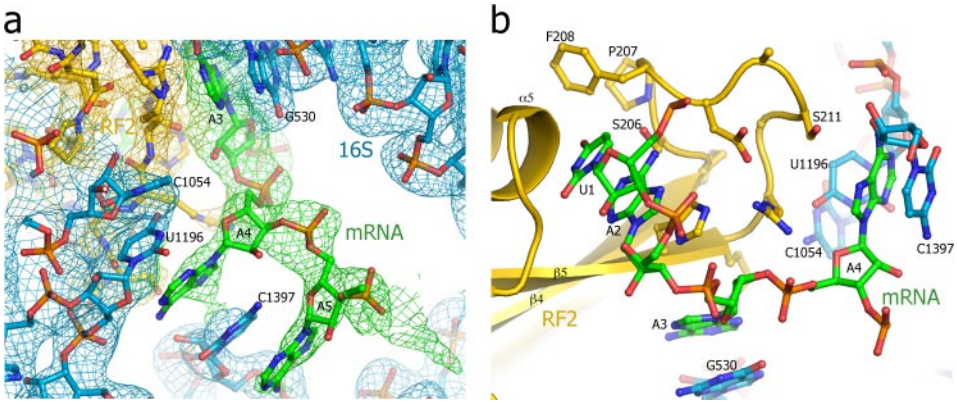

Fig. S4. Interactions of the stop codon and downstream nucleotides (A4 and A5) of mRNA with the ribosome. (*a*) σ_A-weighted $3F_{obs} - 2F_{calc}$ electron density map showing intercalation of A4 between U1196 and C1397 of 16S rRNA (cyan), while C1397 in turn is intercalated between A4 and A5 of mRNA (green). Densities attributed to 16S rRNA and RF2 are contored at 1σ; mRNA at 0.8σ. (*b*) The network of stacking interactions in the decoding center involving stop codon nucleotides and A4.

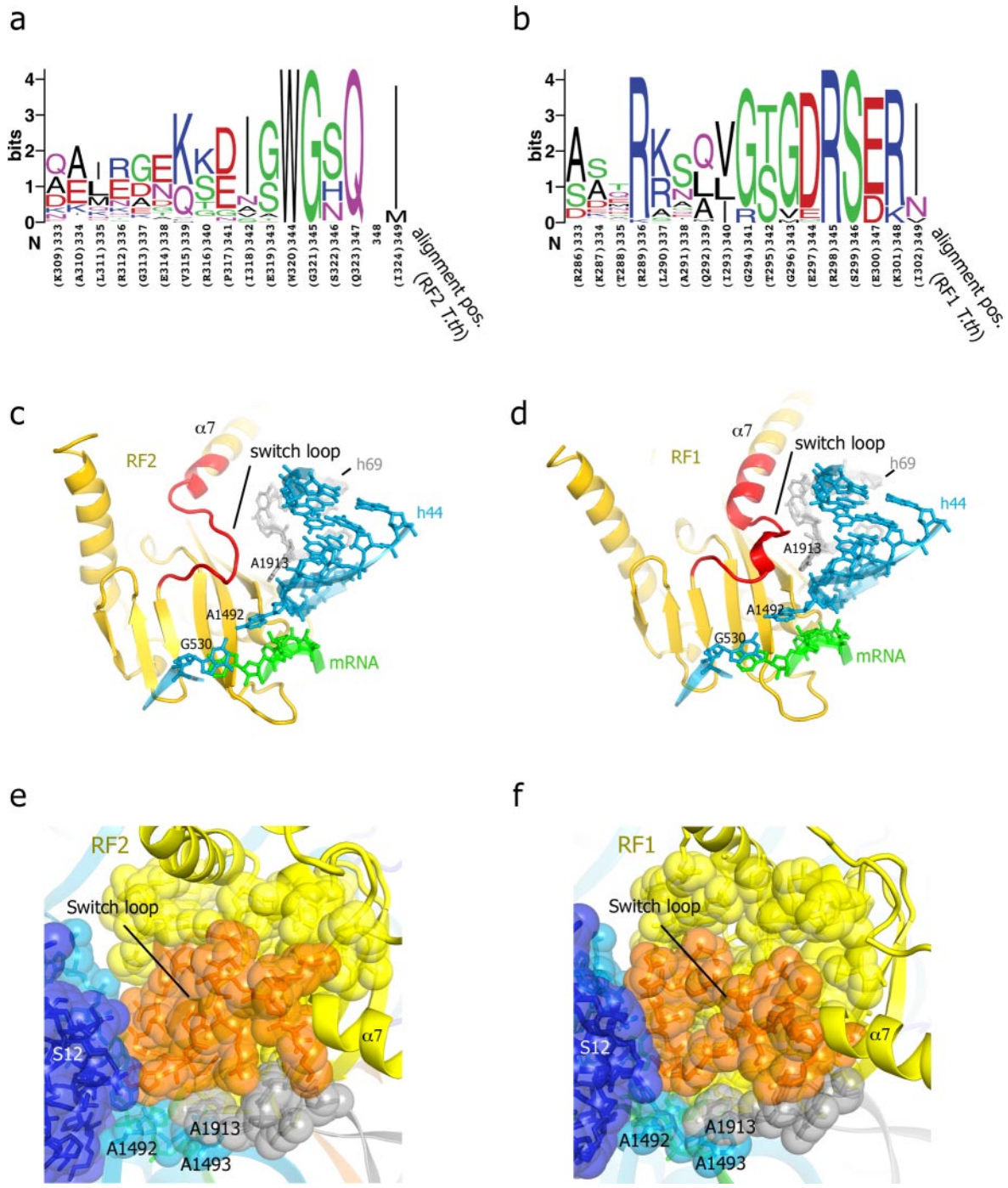

Fig. S5. Sequence divergence and similarity of packing of the switch loops of RF2 (this work) and RF1 (1) at the decoding center of the ribosome. (*a*) Comparison of switch loop sequences between 62 sequences of prokaryotic RF2. (*b*) Comparison of switch loop sequences between 63 sequences of prokaryotic RF1. Positions for alignment between the RF1 and RF2 sequences, and in parentheses, the sequences of *T.th* RF2 and *T.th* RF1, respectively, are given in a and b. Sequence alignments were performed in T-COFFEE (6) and sequence logos generated in SEQLOGO [Crooks GE, Hon G, Chandonia JM, Brenner SE (2004) WebLogo: a sequence logo generator. *Genome Res* 14:1188–1190]. (*c* and *d*) The switch loop of RF2 or RF1 extends helix α7 and packs at the interface of protein S12, A1913 of 23S rRNA and A1492 of 16S rRNA. (*e* and *f*) Packing of the switch loop against the decoding center in the RF2 and RF1-bound complexes, respectively.

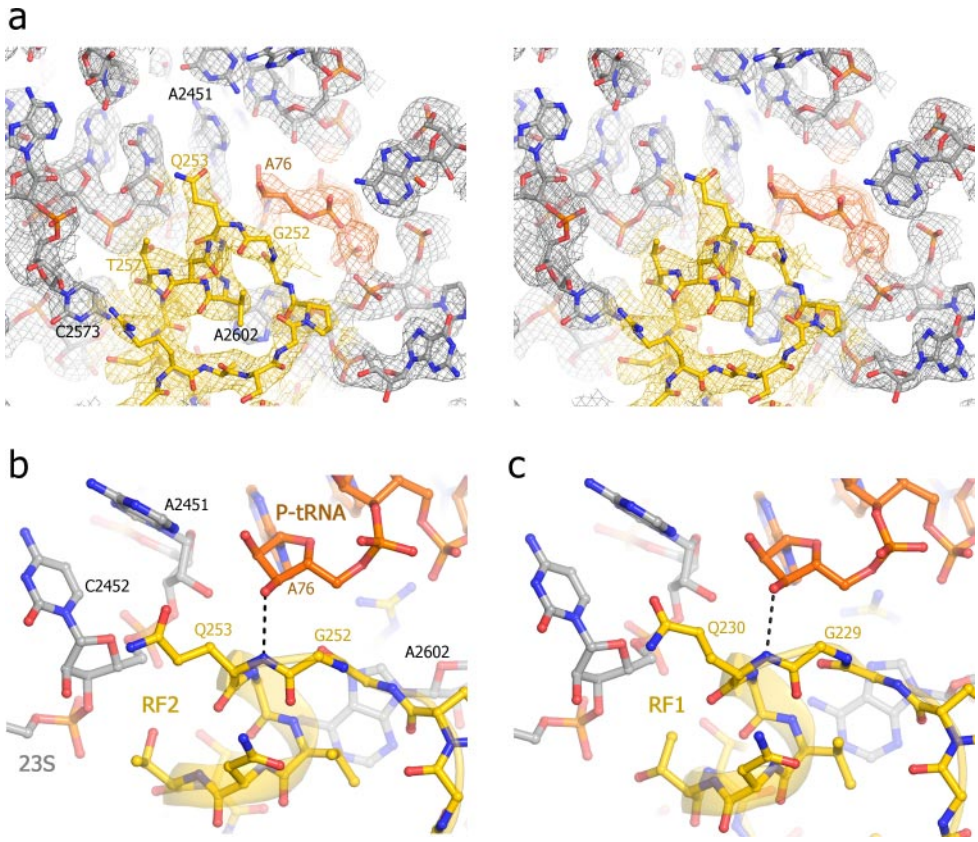

Fig. S6. Interactions of the universally conserved GGQ motif of RF2 (this work) and RF1 (1) in the peptidyl transferase center (PTC) of the termination complex. (*a*) Stereoview of σ_A-weighted $3F_{obs}$-$2F_{calc}$ electron density map for the PTC in the RF2 complex. Densities for RF2 (yellow), P-tRNA (orange) and 23S rRNA (gray) are contoured at 1.7 σ. (*b*) Position of the universally conserved Gln-253 of RF2 in the PTC. (*c*) Position of the universally conserved Gln-230 of RF1 in the PTC.

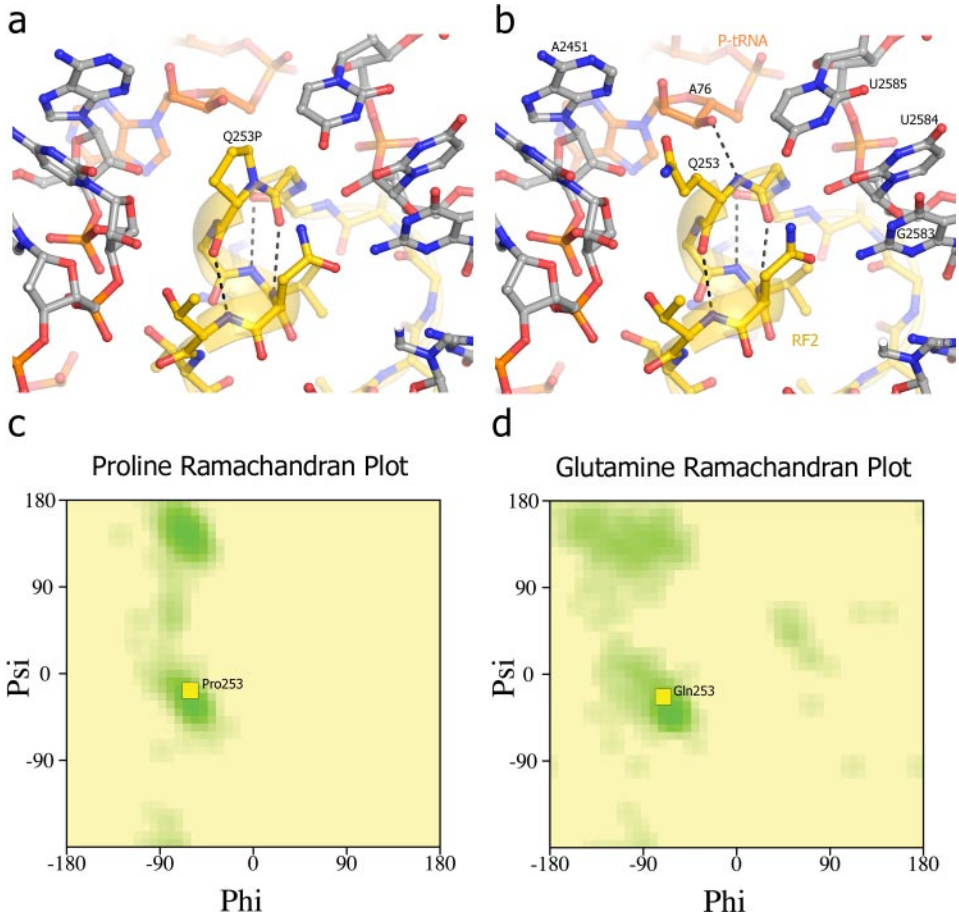

Fig. S7. Conformation of the computationally modeled GGP loop of the Q253P mutant (*a*) is similar to that of the GGQ loop in the crystal structure of (*b*) the RF2 complex (this work), consistent with its stoichiometric binding to the 70S ribosome (Fig. 4*C*). (*c*) Backbone torsion angles (box) for the modeled proline are in a favorable region (green) of the Ramachandran plot and are similar to (*d*) those of glutamine. Ramachandran plots were generated using PROCHECK (4). The *in silico* mutation Q253P was performed in the RF2 termination complex using the mutagenesis option in PyMOL (11) followed by minimization of repulsive van der Waals and geometry energy terms in CNS (9) of all RF2 and 70S ribosome residues within 5Å of each other.

Table S1. Rates of RF1-dependent fMet-tRNA hydrolysis

Release factor	k_{obs}, s^{-1}	
	This work	Shaw and Green, 2007*
RF1 (WT)	>0.03	0.65
Q235A	>0.03	0.18
Q235D	$8.6 \times 10^{-5} \pm 0.8 \times 10^{-5}$	6.8×10^{-5}
Q235N	$25 \times 10^{-5} \pm 0.1 \times 10^{-5}$	8.5×10^{-5}
Q235P	$1.2 \times 10^{-5} \pm 0.09 \times 10^{-5}$	ND
Ribosomes lacking RF1	$1.6 \times 10^{-5} \pm 0.06 \times 10^{-5}$	1.2×10^{-5}

Rates of factor-dependent hydrolysis of fMet-tRNA by mutant *E. coli* RF1 were determined as described in *SI Materials and Methods* and in Shaw JJ, Green R (2007) Two distinct components of release factor function uncovered by nucleophile partitioning analysis. *Mol Cell* 28:458–467. In this work, the rapid reaction rates of wild-type RF1 and the Q235A mutant could not be quantified.

Table S2. X-ray data collection and refinement statistics

Data collection	
Space group	$P2_12_12_1$
Cell dimensions	
a	211.24 Å
b	456.78 Å
c	618.71 Å
α	90°
β	90°
γ	90°
Resolution, Å	50–3.0 (3.11–3.0)*
$R_{p.i.m.}$*	0.097 (0.308)
$I/\sigma I$	8.8 (2.4)
Completeness, %	97.9 (89.9)
Redundancy	16.8 (8.4)
Refinement	
Resolution, Å	50–3.0
No. reflections	1,148,216
R_{work}/ R_{free}	0.280/0.316
No. atoms	301,212
Protein atoms	98,072
RNA atoms	200,748
Ions	2,392
rmsd	
Bond lengths, Å	0.006
Bond angles, °	1.20

The highest-resolution shell is shown in parenthesis.

*$R_{p.i.m.}$ is the precision-indicating merging *R* factor [Weiss MS (2001) Global indicators of X-ray data quality. *J Appl Crystallogr* 34:130–135].